An Efficient Post-Disaster Communication System: Performance Analysis and Optimization

Khaled Alshehri[1], Anas M. Salhab[2], Ali Arshad Nasir[3]

***Abstract*—In this paper, we propose a communication system that is efficient for post-disaster situations such as natural disasters or man-made situations like wars. The proposed system utilizes two new techniques, namely reconfigurable intelligent surfaces (RISs) and unmanned aerial vehicle (UAV) to help the source in sending its message to destination. To investigate the performance of the proposed system, we use accurate closed-form approximations of channel distributions to derive closed-form approximations for the outage probability (OP) and average symbol error probability (ASEP) assuming independent non-identically distributed (i.ni.d.) fading channels. Furthermore, we derive the asymptotic OP at the high signal-to-noise ratio (SNR) regime to get more insights into the system performance. We also study some practical scenarios related to RISs, UAV, and destination locations and illustrate their impact on the system performance through simulations. Finally, we formulate and solve two optimization problems with the objective of minimizing the total OP. The first problem focuses on optimizing the transmit power allocation at both the source and the UAV, while the second problem optimizes the UAV location.**

***Index Terms*—Reconfigurable intelligent surfaces, optimization, unmanned aerial vehicle, performance analysis.**

I. Introduction

Recently, unmanned aerial vehicle (UAV) has received considerable attention as a solution for many wireless communication problems such as network accessing difficulties in remote areas and in places where disasters have occurred. Given the need to improve the performance and coverage of UAV communication systems, many researchers have focused on reconfigurable intelligent surfaces (RISs) as a promising complementary solution. RIS is an artificial surface made of electromagnetic material capable of customizing the propagation of the radio waves impinging upon it [1]- [3]. It represents a new low-cost/less-complicated solution to realize wireless communication with high spectral and energy efficiencies. Mixing these two techniques together can noticeably help in securing wireless communication links in Palestine, especially in war and unstable situations.

Because of the promising potential of RIS technology, it has been recently used to enhance the performance of UAV networks in many studies and under different scenarios. In literature, there are various configurations for RIS-aided UAV systems; either a RIS is installed on the UAV or left stationary. For example, one of the earliest papers on RIS-UAV systems is [4], where a system of a UAV that sends a signal to a receiver aided by stationary RISs was presented. The authors proposed an optimization algorithm to maximize the average achievable rate. In a more recent study, [5] considered a scenario where a source sends a signal to a UAV through a stationary RIS and then to a destination. The ground-to-air (G2A) link between the source and a RIS element was assumed to be Rayleigh distributed, while the channel between the RIS element and UAV was assumed to follow Rician distribution. For the air-to-ground (A2G) link, the authors modeled the signal-to-noise ratio (SNR) statistics with a Noncentral chi-squared distribution. Expressions of the outage probability and bit error rate were derived based on the approximations of the system SNR statistics.

Another example is the work done in [6], where the authors considered a UAV communicating with a vehicle through a RIS with multiple interfering vehicles operating in the same frequency band. The authors analyzed the system performance for finite blocklength (FBL) and infinite BL-based transmissions. [7] is one of the earliest papers that treated the case where RIS is installed on a UAV, where a Q-learning algorithm was used to optimize the downlink communication capacity. In a recent paper [8], the authors developed two different distributions to model the system's SNR statistical distribution. In [9], a UAV-assisted communication system with airborne RIS was considered. A composite fading channel model that accounts for both small-scale fading, modeled by the Weibull distribution, and shadowing, modeled by the Inverse-Gamma distribution, including the effect of correlated shadowing was proposed. The paper showed an improved performance in outage probability, ergodic capacity, and energy efficiency when using airborne RISs compared to traditional relaying techniques, especially in environments with correlated shadowing. In [10], the authors studied a multiple RIS-assisted downlink system with a UAV, with assuming all downlink channels undergo multipath fading along with the existence of a non-zero LoS component and modeling the channel coefficients with a Rician distribution. A strategy for selecting among RISs based on channel gains with imperfect and outdated channel state information was proposed.

Although previous studies did provide important insights into UAV and RIS-aided UAV systems, the multi-RIS-aided UAV networks were not properly studied under the multi-RIS model in [11], where the authors analyzed the statistics of an opportunistic RIS selection model using the Laguerre series approach. Using multiple RISs instead of a single RIS increases the system diversity order when the hop where RISs

[1]Department of Mathematics and Statistics, King Fahd University of Petroleum and Minerals (KFUPM), Dhahran, Saudi Arabia (email:khalid.alshehri5390@alum.kfupm.edu.sa)
[2]Department of Engineering, Bethlehem University, Bethlehem, Palestine (email:asalhab@bethlehem.edu)
[3]Department of Electrical Engineering, King Fahd University of Petroleum and Minerals (KFUPM), Dhahran, Saudi Arabia (email:anasir@kfupm.edu.sa)

978-9950-8599-0-6

are used dominates the system performance.

As mentioned above, we in Palestine suffer from critical situations such as wars. In such situations, the communication systems infrastructure like base stations and towers could be damaged at any time. This shows the critical need for having quick communication links, which can be secured using new efficient techniques such as RIS and UAV. Motivated by the above observations, we propose this research work. The contributions of this paper can be summarized as follows:

- We provide a performance analysis of multi-RIS-aided UAV networks over Nakagami-m fading channels for the source-to-RISs links and Rician fading channel for the UAV-to-destination fading link. To cover more scenarios and to have flexibility in RIS locations between the source and UAV, an independent and non-identically distributed (i.ni.d.) case is considered for RIS channels.
- We derive accurate approximations for the system outage probability (OP) and average symbol error probability (ASEP). The derived expressions are valid for an arbitrary number of reflecting elements and non-integer values of the Nakagami fading parameter.
- We further study the effect of various system parameters such as number of reflecting elements, number of RISs, distances between the source to RIS and RIS to UAV, location of RISs, UAV's height and horizontal distance, etc., on the system performance. They are investigated under realistic conditions, as shown in the Numerical Results Section.
- We also formulate and solve two optimization problems. The first problem optimizes the transmit power allocation at both the source and the UAV under the constraint of a total transmit power budget, with the objective of minimizing the system outage probability. The second problem optimizes the location of the UAV to minimize the outage probability.

A. Paper Organization, Notations, and Symbols

The rest of this paper is organized as follows. Section II presents the system and channel models. The performance analysis is evaluated in Section III. The optimization problem and its solution are presented in Section IV. Simulations and numerical results are discussed in Section V. Finally, the paper is concluded in Section VI.

Notations and symbols: The functions and operators used throughout this paper are provided in Table I.

TABLE I
NOTATIONS USED IN THE PAPER.

Notation	Definition
$P_r[\cdot]$	Probability operator
$F_X(x)$	Cumulative distribution function of a random variable X
$f_X(x)$	Probability density function of a random variable X
$\lvert\cdot\rvert$	Absolute value
$\mathbb{C}^{m\times n}$	Set of matrices with dimension $m \times n$
$(\cdot)^T$	Transpose operator
$\mathbb{E}[\cdot]$	Expectation operator
$Var(\cdot)$	Variance operator
$\Gamma(\cdot)$	Gamma function
$\exp(\cdot)$	Exponential function
$Q(\cdot)$	Q-function
$L_n^{(\alpha)}(\cdot)$	Generalized Laguerre polynomials
$Q_v(\cdot,\cdot)$	Generalized Marcum Q-function
${}_pF_q(\cdot;\cdot;\cdot)$	Generalized hypergeometric function
$I_v(\cdot)$	Modified Bessel function of the first kind
$\Phi_1(.,.,.;.,.)$	Humbert hypergeometric function of the first kind

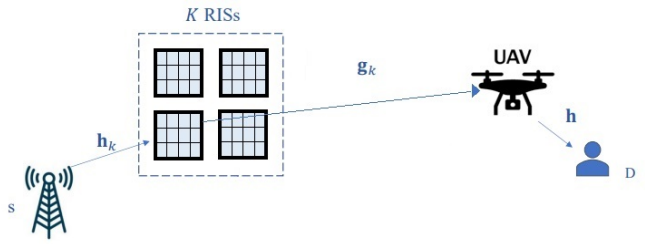

Fig. 1. A multi-RIS aided UAV communication system model.

II. System and Channel Models

As shown in Figure 1, we consider a multi-RIS network that assists the communication between a source and the UAV in the first hop. Only one among the multiple RISs is selected for communication using the opportunistic RIS selection scheme. During the second hop, the UAV forwards the signal to destination using the decode-and-forward (DF) relaying protocol.

This section illustrates the proposed system and channel models of multi-RIS-assisted UAV systems with the RIS selection strategy.

A. Multiple RISs-Assisted G2A Channel

We consider a multi-RIS assisted network, in which a single-antenna source (S) communicates with a UAV assisted by K multiple RISs on the ground. Each RIS, $\{\text{RIS}_k\}_{k=1}^{K}$, is equipped with N_k passive elements. We also assume that the communication between the S and UAV is only provided via RISs and the direct communication links between them are unavailable and no LoS exists between these communicating nodes due to natural or man-made obstacles. An example is when RISs are mounted on the building facets while the source is around that building. In this case, a link between the RISs and the source will be available. However, due to high-rise buildings, the UAV is out of sight from the source and closer to the destination. We assume that the UAV maneuvers to an optimal location and then hovers there to serve the destination, where we later optimize that location.

The S-RIS$_k$ links in the first hop are assumed to undergo Nakagami-m fading with shape parameter $m_{k,1}$ and scale parameter $\Omega_{k,1}$, where the channel vector between the S and RIS$_k$ is denoted by $\mathbf{h}_k \in \mathbb{C}^{N_k\times 1}$, $\mathbf{h}_k = \left[h_k^{(1)},...,h_k^{(i)},...,h_k^{(N_k)}\right]^T$, $h_k^{(i)} = \frac{1}{\sqrt{P_{L,k,1}}}\alpha_k^{(i)}e^{-j\phi_k^{(i)}}$ denotes the channel coefficient between the S and RIS$_k$ ith element, where $P_{L,k,1}$, $\alpha_k^{(i)}$, and $\phi_k^{(i)}$, respectively refer to the path-loss, channel amplitude, and channel phase of the first hop. Likewise, the RIS$_k$-UAV links are also assumed to have Nakagami-m fading channel model with shape parameter $m_{k,2}$ and scale parameter $\Omega_{k,2}$, where the channel vector between the RIS$_k$ and UAV is denoted by $\mathbf{g}_k \in \mathbb{C}^{N_k\times 1}$, $\mathbf{g}_k = \left[g_k^{(1)},...,g_k^{(i)},...,g_k^{(N_k)}\right]^T$, $g_k^{(i)} = \frac{1}{\sqrt{P_{L,k,2}}}\beta_k^{(i)}e^{-j\Phi_k^{(i)}}$

denotes the channel coefficient between ith RIS element and UAV, where $P_{L,k,2}$, $\beta_k^{(i)}$, and $\Phi_k^{(i)}$, respectively refer to the path-loss, channel amplitude, and channel phase of the second hop. The reflection coefficients of the RIS$_k$ are denoted by the entries of the diagonal matrix $\mathbf{\Theta}_k \in \mathbb{C}^{N_k \times N_k}$, for the ith element. Under the full reflection assumption, we have $\Theta_k^{(i,i)} = e^{j\theta_k^{(i)}}$, where $\theta_k^{(i)} \in [0, 2\pi)$. The signal received at UAV from the reflected signals of RIS$_k$ can be expressed as

$$y_k = \sqrt{\frac{E_s}{P_{L,k}}} \sum_{i=1}^{N_k} \alpha_k^{(i)} \beta_k^{(i)} s + n_k, \tag{1}$$

where E_s is the average power of the transmitted signal, s is the transmitted signal, n_k denotes the additive white Gaussian noise (AWGN) sample with zero mean and variance N_0, and $P_{L,k}$ denotes the overall path-loss of the RIS$_k$-assisted path. Here, $P_{L,k} = P_{L,k,1} P_{L,k,2}$ and given by [12]

$$P_{L,k} = \left(\left(\frac{\lambda}{4\pi} \right)^4 \frac{G_{k,1} G_{k,2}}{d_{k,1}^2 d_{k,2}^2} \epsilon_k \right)^{-1}, \tag{2}$$

where λ is the wavelength, $G_{k,1}$ and $G_{k,2}$ are the gains of the RIS$_k$ in the first and second hops, respectively, and ϵ_k is the efficiency of RIS$_k$, which is described as ratio of the transmitted signal power by RIS to the received signal power by RIS. In this paper, it is assumed that $\epsilon_k = 1$. Furthrmore, $d_{k,1}$ and $d_{k,2}$ are the distances from the source-to-RIS$_k$ and RIS$_k$-to-UAV, respectively.

The RIS$_k$ optimizes the phase reflection coefficients to maximize the received SNR at UAV, by aligning the phases of the reflected signals to the sum of the phases of its incoming and outgoing fading channels. Thus, the maximized end-to-end (e2e) SNR for RIS$_k$ can be expressed as [3]

$$\gamma_k = \frac{E_s}{N_0 P_{L,k}} \left(\sum_{i=1}^{N_k} \alpha_k^{(i)} \beta_k^{(i)} \right)^2 = \frac{\overline{\gamma}}{P_{L,k}} Z_k^2, \tag{3}$$

where $\overline{\gamma} = \frac{E_s}{N_0}$ is the average SNR at the receiver.

B. RIS Selection Strategy

In this system, we consider that one out of the K RISs is selected to aid the communications. Specifically, the choice of the suitable RIS is performed to maximize the received signal SNR at the UAV. Therefore, the maximized e2e SNR of the selected RIS can be expressed as

$$\gamma_a = \max_{k=1,\ldots,K} \{\gamma_k\}. \tag{4}$$

Let $a_k = \frac{m_{k,1} m_{k,2} N_k \Gamma(m_{k,1})^2 \Gamma(m_{k,2})^2}{m_{k,1} m_{k,2} \Gamma(m_{k,1})^2 \Gamma(m_{k,2})^2 - \Gamma\left(m_{k,1}+\frac{1}{2}\right)^2 \Gamma\left(m_{k,2}+\frac{1}{2}\right)^2} - N_k$, and $b_k = \frac{m_{k,1} m_{k,2} \Gamma(m_{k,1})^2 \Gamma(m_{k,2})^2 - \Gamma\left(m_{k,1}+\frac{1}{2}\right)^2 \Gamma\left(m_{k,2}+\frac{1}{2}\right)^2}{\sqrt{\frac{m_{k,1}}{\Omega_{k,1}}} \Gamma(m_{k,1}) \Gamma\left(m_{k,1}+\frac{1}{2}\right) \sqrt{\frac{m_{k,2}}{\Omega_{k,2}}} \Gamma(m_{k,2}) \Gamma\left(m_{k,2}+\frac{1}{2}\right)}$. Then, the cumulative distributive function (CDF) and probability density function (PDF) of γ_a can be, respectively given by [11]

$$F_{\gamma_a}(\gamma) = \sum_{n_1=0}^{\infty} \ldots \sum_{n_K=0}^{\infty} \prod_{k=1}^{K} \frac{(-1)^{n_k} \left(\sqrt{\frac{P_{L,k}}{\overline{\gamma}_a b_k^2}} \right)^{a_k+n_k}}{n_k! \left(a_k + n_k\right) \Gamma(a_k)} \times \gamma^{\frac{\sum_{k=1}^{K}(a_k+n_k)}{2}}, \tag{5}$$

$$f_{\gamma^*}(\gamma) = \sum_{j=1}^{K} \frac{\left(\frac{P_{L,j}}{\bar{\gamma}}\gamma\right)^{\frac{a_j-1}{2}} \exp\left(-\sqrt{\frac{P_{L,j}}{\bar{\gamma} b_j^2}\gamma}\right)}{2 b_j^{a_j} \Gamma\left(a_j\right) \sqrt{\frac{\bar{\gamma}}{P_{L,j}}\gamma}} \sum_{k\neq j,k=1}^{\infty} \cdots \sum_{k\neq j,k=K}^{\infty} \tag{6}$$

$$\prod_{k\neq j,k=1}^{K} \frac{(-1)^{n_k} \left(\sqrt{\frac{P_{L,k}}{\bar{\gamma} b_k^2}} \right)^{a_k+n_k}}{n_k! \left(a_k + n_k\right) \Gamma\left(a_k\right)} \times \gamma^{\frac{\sum_{k\neq j,k=1}^{K}(a_k+n_k)}{2}}, \tag{7}$$

where $\Gamma(.)$ is the Euler gamma function. These expressions were derived by approximating the true distribution of γ_k using the first term of the Laguerre series expansion. In this paper, we observe that all infinite series can be truncated to 30–50 terms, while still providing a very good approximation to the exact expressions.

C. A2G Channel

In the second channel, the UAV sends the signal to a destination on ground. We assume that UAV maneuvers to an optimal location (discussed in Section IV) and then hovers there while serving the destination. The signal received at the destination (D) is given by

$$y_b = hx + n_u, \tag{8}$$

where $h = \frac{1}{\sqrt{L}} \chi e^{-j\theta}$ with θ being the phase of the second channel and $n_u \sim \mathcal{CN}(0, N_u)$ denotes the AWGN term. Then, the instantaneous SNR at D is given by

$$\gamma_b = \frac{|\chi|^2 E_u}{N_u L}, \tag{9}$$

where $L = 10 \log_{10}\left(L_0^{\alpha}\right) + A$ is the path-loss [5], E_u is the transmit power of the UAV, $L_0 = \sqrt{h^2 + r_0^2}$ is the distance from UAV to D, where r_0 and h are the UAV's horizontal distance from D and height, respectively. α is the path-loss exponent and it is given by $\alpha = a_1 P_{LoS} + b_1$, where a_1, b_1 are constants determined by the environment and the transmit frequency and P_{LoS} is the line of sight(LoS) probability. χ is the channel amplitude, which follows Rician distribution. Then, the PDF of γ_b can be written as

$$f_{\gamma_b}(\gamma) = \frac{(1+K_0) e^{-K_0} L}{\overline{\gamma_b}} e^{\left(-\frac{1+K_0}{\overline{\gamma_b}} L\gamma\right)} \times I_0\left(2\sqrt{\frac{K_0(1+K_0)}{\overline{\gamma_b}} L\gamma}\right), \tag{10}$$

where $\overline{\gamma_b} = \frac{E_u}{N_u}$, K_0 is the Rician factor and I_0 is the modified Bessel function of the first kind and order zero. The CDF of γ_b is given by [13]

$$F_{\gamma_b}(\gamma) = 1 - Q_1\left(\sqrt{2K_0}, \sqrt{\frac{2\gamma L(1+K_0)}{\overline{\gamma_b}}}\right), \tag{11}$$

where Q_1 is the first order Marcum-Q function. The LoS probability P_{LoS} is modeled as follows [14]

$$P_{LoS}(\theta) = \frac{1}{1 + \beta e^{-b(\theta - a)}}. \tag{12}$$

Also, from [13] we model the Rician factor as $K_0 = a_2 \cdot e^{b_2 \tan^{-1}\left(\frac{h}{r_0}\right)}$, where a_2 and b_2 are constants to be determined later.

III. Performance Analysis

In this section, we derive theoretical expressions for the system outage probability and average symbol error probability. We also derive asymptotic expressions for both performance metrics. These results will be used then to study the diversity order and coding gain of the system.

A. Outage Probability

The OP of each link is given by

$$P_{i,\text{out}} = F_{\gamma_i}(\gamma_{\text{out}}), \tag{13}$$

where $i \in \{a, b\}$. We measure the overall system outage performance by considering the probability that $\min\{\gamma_a, \gamma_b\}$ falls below a predetermined threshold value. Therefore, The total OP is given by

$$P_{\text{out}} = P_{a,\text{out}} + P_{b,\text{out}} - P_{a,\text{out}} P_{b,\text{out}}. \tag{14}$$

Lemma 1. *The asymptotic expression of the OP, when* $\min\{\overline{\gamma_a}, \overline{\gamma_b}\} \to \infty$*, is given by*

$$P_{\text{out}}^{\infty} = \prod_{k=1}^{K} \left(\frac{b_k^2}{\gamma_{out} P_{L,k} \Gamma(a_k)^{-\frac{2}{a_k}}} \overline{\gamma_a} \right)^{-\frac{a_k}{2}} + \frac{e^{-K_0}(1+K_0)\gamma_{out} L}{\overline{\gamma_b}}. \tag{15}$$

Proof: by (14) we have

$$P_{\text{out}}^{\infty} = P_{a,\text{out}}^{\infty} + P_{b,\text{out}}^{\infty} - P_{a,\text{out}}^{\infty} P_{b,\text{out}}^{\infty} \to P_{a,\text{out}}^{\infty} + P_{b,\text{out}}^{\infty}. \tag{16}$$

The asymptotic OP for the first channel can be calculated by $P_{a,\text{out}}^{\infty} = F_{\gamma_a}^{\infty}(\gamma_{\text{out}}) = \prod_{k=1}^{K} F_{\gamma_k}^{\infty}(\gamma_{\text{out}})$. Then, using [15, Eq. (8.354.1)], we get $F_{\gamma_k}^{\infty}(\gamma_{\text{out}}) = \sum_{n_k=0}^{\infty} \frac{(-1)^{n_k} \left(\sqrt{\frac{\gamma_{\text{out}}}{\overline{\gamma_a}} \frac{\gamma_{\text{out}}}{P_{L,k}}} \right)^{a_k+n_k}}{(a_k+n_k) b_k^{a_k+n_k} \Gamma(a_k)}$. As $\overline{\gamma_a} \to \infty$, this expression is only dominated by the first term in summation. Upon considering that, we get $P_{a,\text{out}}^{\infty}$. For the second channel, the Laguerre series of the OP [16, Eq. (8)]: $P_{b,\text{out}} = e^{-K_0} \sum_{i=0}^{\infty} (-1)^{K_0} \frac{L_i^0(K_0)}{\Gamma(i+2)} \left(\frac{\gamma_{\text{out}}(1+K_0)L}{\overline{\gamma_b}} \right)^{i+1}$, by considering the first term the proof is complete. ∎

B. Average Symbol Error Probability

Theorem 1. *The ASEP for each channel can be given by*

$$P_a = \frac{p\sqrt{q}}{2\sqrt{\pi}} \sum_{n_1=0}^{\infty} \cdots \sum_{n_K=0}^{\infty} \prod_{k=1}^{K} \frac{(-1)^{n_k} \left(\sqrt{\frac{P_{L,k}}{\overline{\gamma_a} b_k^2}} \right)^{a_k+n_k}}{n_k! (a_k+n_k) \Gamma(a_k)} \times \frac{1}{q^{\frac{\sum_{k=1}^{K}(a_k+n_k)}{2} + \frac{1}{2}}} \Gamma\left(\frac{\sum_{k=1}^{K}(a_k+n_k)}{2} + \frac{1}{2} \right), \tag{17}$$

$$P_b = \frac{p\sqrt{q}}{2} \sqrt{\frac{\frac{\overline{\gamma}_b}{L}}{q\frac{\overline{\gamma}_b}{L} + K_0 + 1}} e^{-K_0} \times \left[\Phi_1\left(\frac{1}{2}, 1, 1; \frac{K_0+1}{q\frac{\overline{\gamma}_b}{L} + K_0 + 1}, \frac{K_0(K_0+1)}{q\frac{\overline{\gamma}_b}{L} + K_0 + 1} \right) - {}_1F_1\left(\frac{1}{2}; 1; \frac{K_0(K_0+1)}{q\frac{\overline{\gamma}_b}{L} + K_0 + 1} \right) \right], \tag{18}$$

where Φ_1, ${}_1F_1$ *are the Humbert hypergeometric function of the first kind and Kummer hypergeometric function, respectively.* p *and* q *are constants representing the type of modulation.*

Proof: Our results apply for all general modulation formats that have an ASEP expression of the form

$$P_i = E_{\gamma_i}\left[pQ(\sqrt{2q\gamma}) \right], \tag{19}$$

where $Q(\cdot)$ is the Gaussian Q-function. Such modulation formats include binary phase-shift keying (BPSK) ($p = 1, q = 1$) and M-ary PSK ($p = 2, q = \sin\left(\frac{2\pi}{M}\right)$). The ASEP can be obtained as follows [17]

$$P_i = \frac{p\sqrt{q}}{2\sqrt{\pi}} \int_0^{\infty} \frac{e^{-q\gamma}}{\sqrt{\gamma}} F_{\gamma_i}(\gamma) d\gamma. \tag{20}$$

For P_a, inserting (5) in (20) gives

$$P_a = \frac{p\sqrt{q}}{2\sqrt{\pi}} \sum_{n_1=0}^{\infty} \cdots \sum_{n_K=0}^{\infty} \prod_{k=1}^{K} \frac{(-1)^{n_k} \left(\sqrt{\frac{P_{L,k}}{\overline{\gamma}_b b_k^2}} \right)^{a_k+n_k}}{n_k! (a_k+n_k) \Gamma(a_k)} \times \int_0^{\infty} \gamma^{\frac{\sum_{k=1}^{K}(a_k+n_k)}{2} - \frac{1}{2}} e^{-q\gamma} d\gamma. \tag{21}$$

With the help of $\int_0^{\infty} x^{v-1} e^{-\mu x} dx = \frac{1}{\mu^v}\Gamma(v)$ [15, Eq. (3.381.4)], we obtain (17).
For P_b, inserting (11) in (20) and using [18, Eq. (3)] we obtain (18) and the proof is complete. ∎

Corollary 1. *The asymptotic ASEP for each channel can be given by*

$$P_a^{\infty} = \frac{p}{2\sqrt{\pi}} \prod_{k=1}^{K} \frac{\left(\sqrt{\frac{P_{L,k}}{\overline{\gamma_a} b_k^2}} \right)^{a_k}}{a_k \Gamma(a_k)} \frac{\Gamma\left(\frac{\sum_{k=1}^{K} a_k}{2} + \frac{1}{2} \right)}{q^{\frac{\sum_{k=1}^{K} a_k}{2}}}, \tag{22}$$

$$P_b^{\infty} = \frac{p(K_0+1)e^{-K_0}}{4(q\frac{\overline{\gamma_a}}{L} + K_0 + 1)}. \tag{23}$$

Proof: For P_a^{∞}, using (17) as $\overline{\gamma_a} \to \infty$, the expression is dominated by the first term. Taking the first term yields the desired asymptotic expression. For P_b^{∞}, using (18) and the series representation of both the Humbert and Kummer hypergeometric function, as $\overline{\gamma_b} \to \infty$ the series are dominated by the first few terms. Taking the first two terms of Kummer hypergeometric function and the first three terms (the less than quadratic terms) of the Humbert hypergeometric function will yield $\frac{p\sqrt{q}(K_0+1)e^{-K_0}}{4(q\frac{\overline{\gamma_a}}{L} + K_0 + 1)^{\frac{3}{2}}} \sqrt{\frac{\overline{\gamma_a}}{L}}$. Simplifying and using the fact that $\frac{\frac{\overline{\gamma_a}}{L}}{q\frac{\overline{\gamma_a}}{L} + K_0 + 1} \to \frac{1}{q}$ yields the desired expression. ∎

For a dual-hop DF relaying communication system, the ASEP is given by [19]

$$P_e = P_a + P_b - 2P_aP_b. \tag{24}$$

Upon substituting (17) (or (22)) & (18) (or (23)) into (24), we get the overall system ASEP.

IV. Optimization

In this section, we formulate and solve the following two optimization problems:

A. Optimal transmit power

Given a total transmit power budget E_T, what is the optimal transmit power for the first and second channels that minimizes the total outage probability? More precisely our problem can be formulated as follows

$$\begin{array}{ll}\text{minimize} & P_{\text{out}}^{\infty}(E_s, E_u),\\ \text{subject to} & E_s + E_u \leq E_T,\end{array}$$

where P_{out}^{∞} is the asymptotic outage probability in (15). Set $M \triangleq \sum_{k=1}^{K} a_k$, $c_1 \triangleq N_0^{M/2} \prod_{k=1}^{K} \left(\frac{b_k^2}{\gamma_{\text{out}} P_{L,k} \Gamma(a_k)^{-\frac{2}{a_k}}}\right)^{-\frac{a_k}{2}}$, $c_2 \triangleq N_u e^{-K_0} (1+K_0)\gamma_{\text{out}} L$ and $d \triangleq [\frac{2c_2}{Mc_1}]^{\frac{-1}{M/2+1}}$, we get

$$P_{\text{out}}^{\infty}(E_s, E_u) = c_1 E_s^{-M/2} + c_2 E_u^{-1}. \tag{25}$$

This function is convex. To find the minimum outage probability, let us define the Lagrangian

$$\mathcal{L}(E_S, E_u) = c_1 E_s^{-M/2} + c_2 E_u^{-1} + \mu(E_s + E_u - E_T),$$

where μ is the Lagrangian parameter. By setting the partial derivatives of $\mathcal{L}(E_S, E_u)$ to zero with respect to E_s, E_u, and μ, we get the following system of equations

$$\begin{aligned} E_s &= \left(\frac{2\mu}{Mc_1}\right)^{-\frac{1}{\frac{M}{2}+1}},\\ E_u &= \sqrt{\frac{c_2}{\mu}},\\ E_s + E_u &= E_T. \end{aligned}$$

This leads to the equation $E_s = d(E_T - E_s)^{\frac{4}{M+2}}$, which can be solved numerically. Therefore, if x^* solves $x = d(E_T - x)^{\frac{4}{M+2}}$, then our desired solution is $E_s = x^*, E_u = E_T - x^*$.

B. Optimal UAV's location

Let the source S be placed at $(0,0,0)$, the RIS$_i$ at $(x_i, y_i, 0)$, and the destination D at $(x_d, 0, 0)$. What is the optimal placement of the UAV that minimizes the outage probability? This problem is highly non-convex. Thus, to make the problem more tractable, we will restrict the problem to the circle centered around D with a fixed height h. That is the problem can be reformulated as follows

$$\begin{array}{ll}\text{minimize} & P_{\text{out}}^{\infty},\\ \text{subject to} & (x-x_d)^2 + y^2 = r_0^2, z = h.\end{array}$$

Since r_0 and h are constants, then $P_{b,\text{out}}^{\infty}$ is constant too. But, $P_{a,\text{out}}^{\infty} = \prod_{k=1}^{K} \left(\frac{b_k^2}{\gamma_{\text{out}}\Gamma(a_k)^{-\frac{2}{a_k}}\overline{\gamma_a}}\right)^{-\frac{a_k}{2}} P_{L,k}^{\frac{a_k}{2}}$ and $P_{L,k} = \left(\left(\frac{\lambda}{4\pi}\right)^4 \frac{G_{k,1}G_{k,2}}{d_{k,1}^2}\epsilon_k\right)^{-1} d_{k,2}^2$. Therefore, $P_{a,\text{out}}^{\infty} = c_0 \prod_{k=1}^{K} d_{k,2}^{a_k}$, where c_0 is a constant and $d_{k,2}^2 = (x-x_k)^2 + (y-y_k)^2 + h^2$. The outage probability can now be written as $c_0 \prod_{k=1}^{K} d_{k,2}^{a_k} + c_1$. Then we can reformulate the problem as follows

$$\begin{array}{ll}\text{minimize} & \prod_{k=1}^{K} d_{k,2}^{a_k},\\ \text{subject to} & (x-x_d)^2 + y^2 = r_0^2, z = h,\end{array}$$

where r_0 and h are constants. To solve this problem, we can solve the following equivalent problem

$$\begin{array}{ll}\text{minimize} & \sum_{k=1}^{K} \frac{a_k}{2} * \ln((x-x_k)^2 + (y-y_k)^2 + h^2),\\ \text{subject to} & (x-x_d)^2 + y^2 = r_0^2, z = h.\end{array}$$

Set $z_i = (x-x_i)^2 + (y-y_i)^2 + h^2$ so we get the function $\sum_{k=1}^{K} \frac{a_k}{2} * \ln(z_i)$. Then, when linearizing this function at a point $\overline{z_i} = (x'-x_i)^2 + (y'-y_i)^2 + h^2$ we get the following problem

$$\begin{array}{ll}\text{minimize} & \sum_{k=1}^{K} a_k * (\ln(\overline{z_i}) + \frac{1}{\overline{z_i}}(z_i - \overline{z_i})),\\ \text{subject to} & (x-x_d)^2 + y^2 = r_0^2, z = h.\end{array}$$

Therefore, we can solve our original problem by solving the linearized problem iteratively until it converges to the desired minimal solution as it is illustrated in Algorithm 1 below.

Algorithm 1 Algorithm for solving the optimization problem

Input $(x_i, y_i), a_i$ for $i = 1, .., K, x_d, h$ and r_0
Output: (x^*, y^*)

Set $x_{min}(0) \triangleq x_d, y_{min}(0) \triangleq r_0$.
For $i = 1, \cdots, K$, $z_i(0) = (x_{min}(0) - x_i)^2 + (y_{min}(0) - y_i)^2 + h^2$.
Repeat until convergence of $\vec{z}(k)$,
Set $s \triangleq \sum_{i=1}^{K} \frac{a_i y_i}{z_i(k)}, q \triangleq |2x_d \sum_{i=1}^{K} \frac{a_i}{z_i(k)} - 2\sum_{i=1}^{K} \frac{a_i x_i}{z_i(k)}|$.
Set $v \triangleq x_d - \frac{r_0 q}{\sqrt{4s^2+q^2}}, v' \triangleq x_d + \frac{r_0 q}{\sqrt{4s^2+q^2}}$.
Set $f \triangleq r_0\sqrt{1 - \frac{q^2}{4s^2+q^2}}, f' \triangleq -r_0\sqrt{1 - \frac{q^2}{4s^2+q^2}}$.
If $\sum_{i=1}^{K} \frac{a_i(v-x_i)^2}{z_i(k)} \leq \sum_{i=1}^{K} \frac{a_i(v'-x_i)^2}{z_i(k)}$
Then $x_{min}(k+1) = v$
Else $x_{min}(k+1) = v'$.
If $\sum_{i=1}^{K} \frac{a_i(f-y_i)^2}{z_i(k)} \leq \sum_{i=1}^{K} \frac{a_i(f'-y_i)^2}{z_i(k)}$.
Then $y_{min}(k+1) = f$.
Else $y_{min}(k+1) = f'$.
For $i = 1, \cdots, K$, $z_i(k+1) = (x_{min}(k+1) - x_i)^2 + (y_{min}(k+1) - y_i)^2 + h^2$. Reset $k \leftarrow k+1$.
Output $x^* = \lim_{k\to\infty} x_{min}(k)$, $y^* = \lim_{k\to\infty} y_{min}(k)$.

The complexity of the solution used in Algorithm 1 is $O(K + (K+8)/\eta)$, where $\eta = 10^{-3}$ is the precision accuracy for the stopping criteria.

V. Numerical Results

In this section, we present numerical results corresponding to the considered multiple RISs-UAV system. We also validate the theoretical analysis using Monte-Carlo simulations.

Unless otherwise stated, in all presented illustrations, the carrier frequency is assumed to be $f_c = 2$ GHz, the gains of the RISs in the first and second hops are, respectively given as $G_{k,1} = G_{k,2} = 5$ dBi, $\gamma_{\text{out}} = 0$ dB, and $A = 1$ [5].

In Figure 2, we validate the analytical results by comparing them with simulations. In this figure, the outage probability is plotted against the average SNR. We can observe that simulations (asterisks) match the analytically derived results well. Furthermore, we can see that the asymptotic expressions,

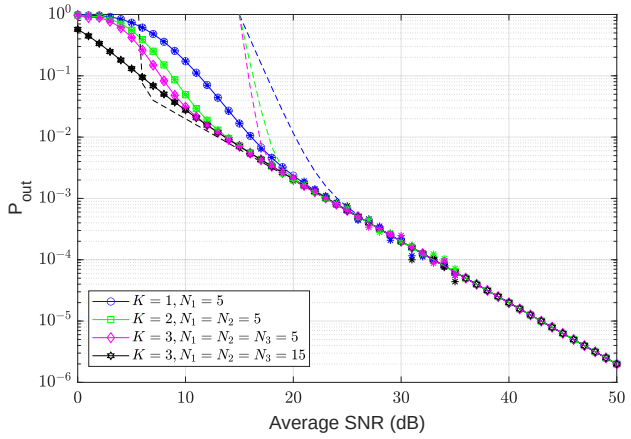

Fig. 2. The outage probability versus average SNR with different numbers of RIS $K \in \{1, 2, 3\}$ and reflecting RIS elements $N_1, N_2, N_3 \in \{5, 15\}$, $(m_{k,1}, m_{k,2}) = (1, 1)$, $(\Omega_{k,1}, \Omega_{k,2}) = (1, 1)$, and $K_0 = 4.77$ dB.

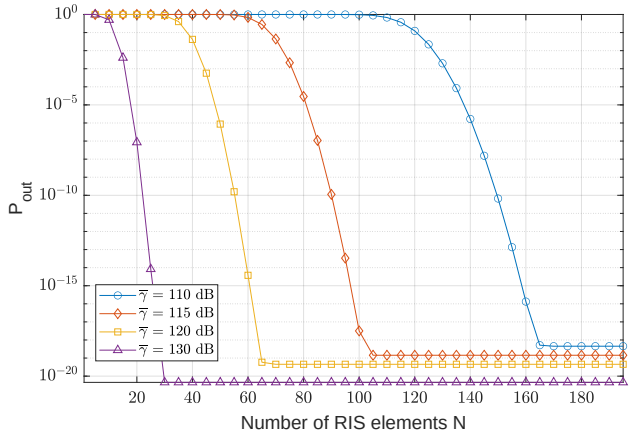

Fig. 4. Outage probability versus number of elements for different average SNRs, $\overline{\gamma_a} = \overline{\gamma_b} = \overline{\gamma}$, $K = 3$, $N_1 = N_2 = N_3 = 5$, $(m_{k,1}, m_{k,2}) = (1, 1)$, $(\Omega_{k,1}, \Omega_{k,2}) = (1, 1)$, and $K_0 = 4.77$ dB.

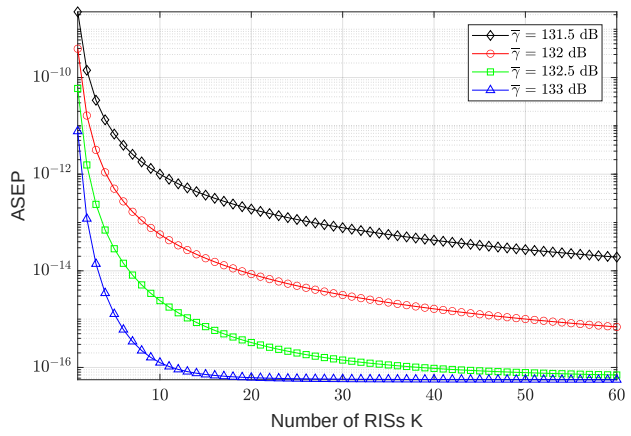

Fig. 3. Average symbol error probability versus the number of RISs for different average SNRs, $\overline{\gamma_a} = \overline{\gamma_b} = \overline{\gamma}$, $K = 3$, $N_1 = N_2 = N_3 = 5$, $(m_{k,1}, m_{k,2}) = (1, 1)$, $(\Omega_{k,1}, \Omega_{k,2}) = (1, 1)$, and $K_0 = 4.77$ dB.

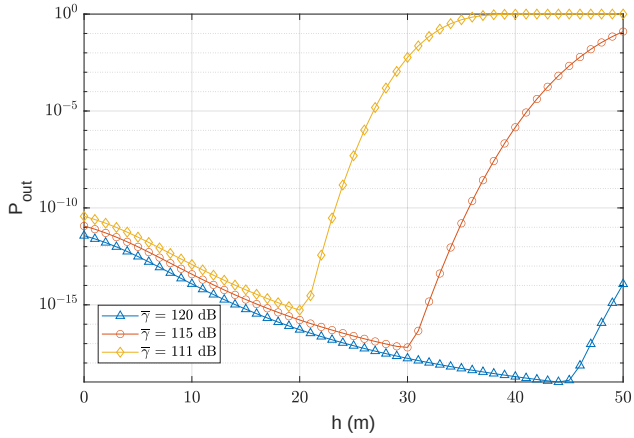

Fig. 5. The outage probability vs the UAV's height for different average SNRs, $\overline{\gamma_a} = \overline{\gamma_b} = \overline{\gamma}$, $K = 3$, $N_1 = N_2 = N_3 = 5$, $(m_{k,1}, m_{k,2}) = (1, 1)$, $(\Omega_{k,1}, \Omega_{k,2}) = (1, 1)$, and $K_0 = 4.77$ dB.

which are plotted as dashed lines, converge to the exact expressions at high SNR values. It is also obvious that all curves converge asymptotically to the same line. This happens when the second channel's outage probability, which decreases as $1/\gamma$ dominates the system performance. It is clear from this figure that a higher number of RISs and reflecting elements enhances the system performance, as expected.

To further investigate the effect of the number of RISs K and number of their elements N on the system performance, Figures 3 and 4 plot the average symbol error probability and outage probability against number of RISs K and number of elements N, respectively. The figures show that the higher the number of RISs or reflecting elements, the better the achieved performance. However, we can see that after a certain number of RISs or reflecting elements, the average symbol error probability or outage probability will be unaffected by changing the two parameters. This is because increasing K and N enhances the performance of the first hop but not the second hop, and so after some numbers, K_{th} and N_{th}, the second hop starts dominating the system performance. The numbers K_{th} and N_{th}, as well as the outage limit, depend on the second hop and other system parameters such as $\overline{\gamma}$.

Figure 5 demonstrates the effect of the UAV's height on the system performance. The outage probability is plotted against the height of the UAV, assuming an urban environment. It is clear that the outage probability decreases at first as the height increases. However, the outage probability starts increasing at some point, creating an optimal height. Here, we analyze the behavior of the first and second hops separately. Initially, as the height increases, the Rician factor increases, hence, enhancing the second hop channel. But, for large elevation, the Rician factor will reach a limit, mainly $a_2 \cdot e^{b_2 \frac{\pi}{2}}$ and will not increase further. So the path-loss effect will dominate, and the second hop outage probability will increase. However, for the first hop, the outage probability increases with the height indefinitely. Thus, the optimal height of the system will be

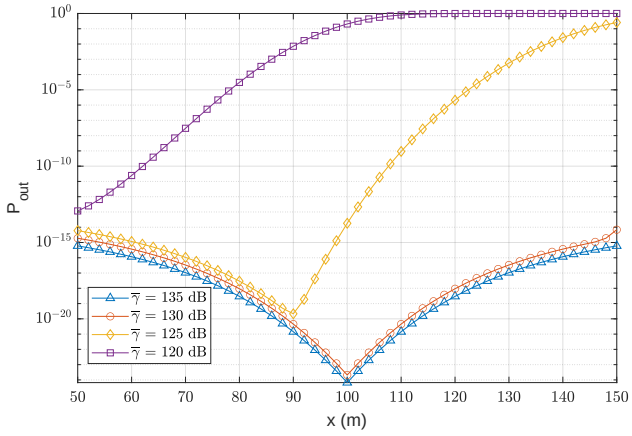

Fig. 6. The outage probability vs the UAV's horizontal position for different average SNRs, $\overline{\gamma_a} = \overline{\gamma_b} = \overline{\gamma}$, $K = 3$, $N_1 = N_2 = N_3 = 5$, $(m_{k,1}, m_{k,2}) = (1,1)$, $(\Omega_{k,1}, \Omega_{k,2}) = (1,1)$, and $K_0 = 4.77$ dB.

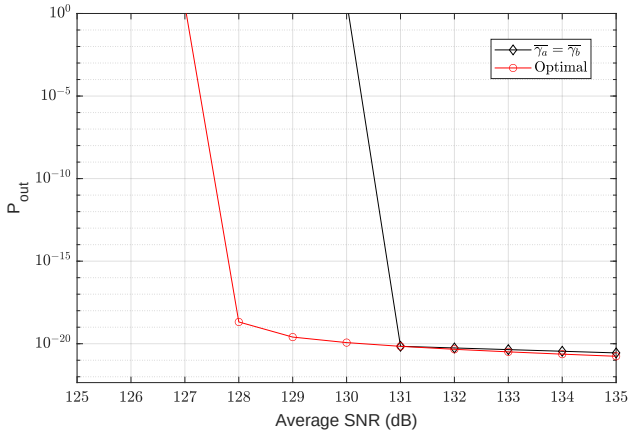

Fig. 7. The outage probability vs total average SNR $\overline{\gamma_T}$ for an optimal choice of E_s, E_u and when $E_s = E_u$, $Nu = N_0$, $K = 3$, $N_1 = N_2 = N_3 = 100$. $(m_{k,1}, m_{k,2}) = (1,1)$, $(\Omega_{k,1}, \Omega_{k,2}) = (1,1)$, and $K_0 = 4.77$ dB.

either at the point where the dominance shifts to the first hop or at the optimal height of the second hop. In these figures, the optimal height is at the shifts. Usually, the optimal height occurs at the point where the dominance shifts. This happens when the optimal point is lower than the second hop's optimal height, and the outage probability at this point is higher.

Figure 6 shows the behavior of the system when the UAV moves horizontally. Here, the destination is placed 100 m away from the source, and the UAV is at a 50 m height. The outage probability is plotted against the horizontal distance of the UAV from the source. We can see that there is an optimal point where the outage probability is at its lowest value. To understand this behavior, notice that moving away from the source increases the outage probability of the first hop, and moving away from the destination increases the outage probability of the second hop and vice versa. Thus, the first hop has an optimal position when the UAV is above the source, and the second hop has an optimal position when the UAV is above the destination. Therefore, the optimal position of the total system occurs either at the point where the dominance shifts (in diamonds) or at the source where the first hop is always dominant (in squares), or at the destination where the second hop is always dominant (in circles and triangles).

Figures 7 and 8 present the optimization results. Figure 7 plots the outage probability against the total average SNR for the optimal and equal transmit power distributions. We can see from this figure that the optimal solution significantly decreases the outage probability. In Figure 8, as the second hop dominates the system performance, its share increases rapidly as the total power increases, in contrast to the first hop, where the increase is slow.

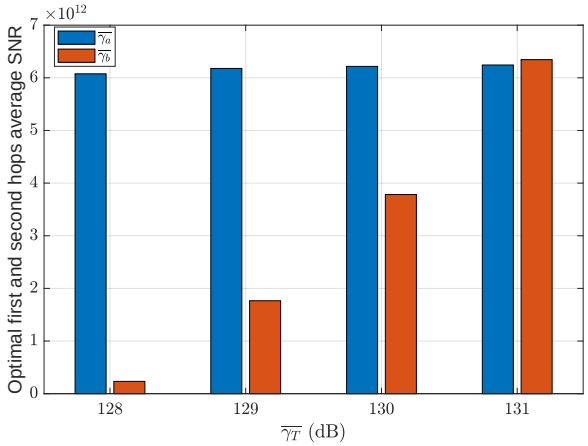

Fig. 8. The optimal channels average SNR vs total average SNR, $N_u = N_0$, $K = 3$, $N_1 = N_2 = N_3 = 100$. $(m_{k,1}, m_{k,2}) = (1,1)$, $(\Omega_{k,1}, \Omega_{k,2}) = (1,1)$, and $K_0 = 4.77$ dB.

VI. Conclusion

In this paper, the performance of a multiple reconfigurable intelligent surfaces-aided dual-hop UAV communication system was studied over Nakagami-m fading channels for the first hop and Rician fading channel for the second hop. Accurate closed-form approximations were first derived for each channel distribution and then used in deriving closed-form approximations for the outage and average symbol error probabilities. Furthermore, an asymptotic expression was derived for the outage probability at the high signal-to-noise ratio regime to get more insights into the system performance. Results showed that multiple RISs could improve the performance and coverage of the UAV communication systems. Finally, we formulated and solved an optimization problem for the transmit power of each channel. One of the possible future research extension is to incorporate UAV trajectory design (its optimal maneuvering).

References

[1] M. Di Renzo *et al.*, "Reconfigurable intelligent surfaces vs. relaying: Differences, similarities, and performance comparison," *IEEE Access*, vol. 1, pp. 798–807, 2020.

[2] M. Di Renzo *et al.*, "Smart radio environments empowered by reconfigurable intelligent surfaces: How it works, state of research, and the road ahead," *IEEE J. Sel. Areas Commun.*, vol. 38, no. 11, pp. 2450–2525, Nov. 2020.

[3] E. Basar, M. Di Renzo, J. De Rosny, M. Debbah, M.-S. Alouini, and R. Zhang, "Wireless communications through reconfigurable intelligent surfaces," *IEEE Access*, vol. 7, pp. 116753–116773, 2019.

[4] S. Li, B. Duo, X. Yuan, Y.-C. Liang, and M. Di Renzo, "Reconfigurable intelligent surface assisted UAV communication: Joint trajectory design and passive beamforming," *IEEE Wire. Commun. Lett.*, vol. 9, no. 5, pp. 716–720, May 2020.

[5] L. Yang, F. Meng, J. Zhang, M. O. Hasna, and M. Di Renzo, "On the performance of RIS-assisted dual-hop UAV communication systems," *IEEE Trans. Veh. Technol.*, vol. 96, no. 9, pp. 10385–10390, Sept. 2020.

[6] N. Agrawal, A. Bansal, K. Singh, and C.-P. Li, "Performance evaluation of RIS-assisted UAV-enabled vehicular communication system with multiple non-identical interferers," *IEEE Trans. Intell. Transp. Syst.*, pp. 1–12, Nov. 2021.

[7] Q. Zhang, W. Saad, and M. Bennis. "Reflections in the sky: Millimeter wave communication with UAV-carried intelligent reflectors," *in Proc. of the 2019 IEEE Global Commun. Conf. (GLOBECOM)*, pp. 1–6, 2019.

[8] L. Yang, P. Li, F. Meng, and S. Yu, "Performance analysis of RIS-assisted UAV communication systems," *IEEE Trans. Veh. Technol.*, vol. 71, no. 8 pp. 9078–9082, May. 2022

[9] Bithas, P. S., Ropokis, G. A., Karagiannidis, G. K., and Nistazakis, H. E, "Uav-assisted communications with ris: A shadowing-based stochastic analysis," *IEEE Trans. Veh. Technol..*, vol. 73, no. 7, pp. 10000-10010, July. 2024.

[10] Bansal, A., Agrawal, N., Singh, K., Li, C. P., and Mumtaz, S, "RIS selection scheme for UAV-based multi-RIS-aided multiuser downlink network with imperfect and outdated CSI," *IEEE Trans. Commun.*, vol. 71, no. 8, pp. 14650–4664, Aug. 2023.

[11] M. Aldababsa, A. M. Salhab, A. A. Nasir, M. H. Samuh, and D. B. da Costa, "Multiple RISs-aided networks: Performance analysis and optimization," *IEEE Trans. Veh. Technol.*, vol. 72, no. 6, pp. 7545–7559, Jun. 2023.

[12] I. Yildirim, A. Uyrus, and E. Basar, "Modeling and analysis of reconfigurable intelligent surfaces for indoor and outdoor applications in future wireless networks," *IEEE Trans. Commun.*, vol. 69, no. 2, pp. 1290–1301, Feb. 2021.

[13] M. M. Azari, F. Rosas, K. -C. Chen, and S. Pollin, "Ultra reliable UAV communication using altitude and cooperation diversity," *IEEE Trans. Wire. Commun.*, vol. 66, no. 1, pp. 330–344, Jan. 2018.

[14] A. Al-Hourani, S. Kandeepan, and S. Lardner, "Optimal LAP altitude for maximum coverage," *IEEE Wire. Commun. Lett.,*, vol. 3, no. 6, pp. 569–572, Dec. 2014.

[15] I. S. Gradshteyn and I. M. Ryzhik, *Tables of Integrals, Series and Products*, 6th ed., San Diago: Academic Press, 2000.

[16] S. Andras, A. Baricz, and Y. Sun, "The generalized Marcum Q-function: An orthogonal polynomial approach," *Acta Universitatis Sapientiae Mathematica*, vol. 3, no. 1, pp. 60–76, Oct. 2011.

[17] M. R. McKay, A. L. Grant, and I. B. Collings, "Performance analysis of MIMO-MRC in double-correlated Rayleigh environments," *IEEE Trans. Commun.*, vol. 55, pp. 497–507, Mar 2007.

[18] P. C. Sofotasios, S. Muhaidat, G. K. Karagiannidis, and B. S. Sharif, "Solutions to integrals involving the Marcum Q-function and applications," *IEEE Signal Proc. Lett.*, vol. 22, no. 10, pp. 1752–1756, Oct. 2015.

[19] O. M. S. Al-Ebraheemy, A. M. Salhab, A. Chaaban, S. A. Zummo, and M.-S. Alouini, "Precise performance analysis of dual-hop mixed RF/Unified-FSO DF relaying with heterodyne detection and two IMDD channel models," *IEEE Photonics J.*, vol. 11, no. 1, pp. 1–22, 2019.

[20] S. Primak, V. Kontorovich, and V. Lyandres, Stochastic Methods and their Applications to Communications: *Stochastic Differential Equations Approach*, West Sussex, U.K.: Wiley, 2004.

[21] G. K. Karagiannidis, N. C. Sagias, and P. T. Mathiopoulos, "$N*$Nakagami: A novel stochastic model for cascaded fading channels," *IEEE Trans. Commun.*, vol. 55, no. 8, pp. 1453–1458, 2007.

[22] N. Bhargav, C. R. N. da Silva, Y. J. Chun, J. Leonardo, S. L. Cotton, and M. D. Yacoub, "On the product of two κ-μ random variables and its application to double and composite fading channels," *IEEE Trans. Wire. Commun.*, vol. 17, no. 4, pp. 2457–2470, 2018.

[23] P. Shankar, "Error rates in generalized shadowed fading channels," *Wireless Pers. Commun.*, vol. 28, pp. 233–238, 2004.

[24] M. Abramowitz and I. A. Stegun, *Handbook of Mathematical Functions with Formulas, Graphs, and Mathematical Tables*, 9th ed., New York, NY, USA: Dover, 1972.

[25] F. W. J. Olver, D. W. Lozier, R. F. Boisvert, and C. W. Clark (eds.), *NIST Handbook of Mathematical Functions*, U.S. Department of Commerce, National Institute of Standards and Technology, Washington, DC; Cambridge University Press, Cambridge, 2010.

[26] A. Annamalai and C. Tellambura, "A simple exponential integral representation of the generalized Marcum Q-function QM (a, b) for real-order M with applications," *in Proc. 54th IEEE MILCOM,* 2008, pp. 1–7.